Visualization of transport-related configurations of the nuclear pore transporter

Christopher W. Akey
MRC Laboratory of Molecular Biology, Cambridge CB2 2QH United Kingdom; and Department of Cell Biology, Stanford University School of Medicine, Stanford, California 94305 USA

ABSTRACT The transport of macromolecules between the cytoplasm and nucleus of the cell is mediated by the nuclear pore complex (NPC). In this study, details of the central transporter assembly within NPCs have been examined by cryoelectron microscopy, image processing, and classification analysis. The NPC transporter in isolated amphibian nuclei appears to adopt a minimum of four transport-related configurations including: (*a*) a putative closed form with a 90–100 Å diameter central pore, (*b*) a docked form with material aligned over the pore, (*c*) an open form with substrates apparently caught "in transit," and (*d*) an open form with an enlarged pore. This data confirms previous observations on NPC transporters labeled with nucleoplasmin-gold (Akey, C. W., and D. S. Goldfarb. 1989. *J. Cell Biol.* 109:971–982) and allows a working model of the central NPC transporter to be proposed. The model is comprised of two supramolecular irislike assemblies which open asynchronously to provide an expanded pore for translocation while maintaining transport fidelity.

INTRODUCTION

The nuclear pore complex (NPC) spans the nuclear envelope and appears to mediate the transfer of ions, small molecules and macromolecules between the cytoplasm and nucleus (for recent reviews see Dingwall and Laskey, 1986; Newport and Forbes, 1987; Gerace and Burke, 1988). The pore complex possesses a striking triple-ring architecture with eightfold symmetry and is comprised of a radially-aligned spoke assembly which is framed top and bottom by two thin coaxial rings (Unwin and Milligan, 1982; Akey, 1989*a*). The NPC has a measured molecular weight of ~124 MD (Reichelt et al., 1990) and is estimated to contain up to 100 different proteins (Gerace and Burke, 1988). Transport of large macromolecules has been shown to occur at the center of the NPC (Stevens and Swift, 1966; Franke, 1974; Feldherr et al., 1984) through a channel-like assembly termed the NPC transporter (Akey and Goldfarb, 1989), which was formerly identified as a central granule or plug (Franke, 1974; Unwin and Milligan, 1982).

Transport mediated by the NPC is bidirectional (Dworetzky and Feldherr, 1988) as exemplified by the specific import of large nuclear proteins (DeRobertis et al., 1978; Dingwall et al., 1982; Kalderon et al., 1984) and the export of preribosomal subunits (see Hadjiolov, 1985), m-RNPs (Stevens and Swift, 1966; Franke, 1974) and t-RNAs (Zasloff, 1983). A passive diffusion pore of ~90 Å diameter has been measured in *Xenopus* nuclei and attributed to the NPC (Paine et al., 1975). Therefore, the NPC probably mediates the passive transfer of ions, small molecules, and macromolecules of less than ~40 kD across the nuclear envelope (Paine, 1975; Peters, 1984). However, recent work by Breeuwer and Goldfarb (1990) suggests that the entry of histone H1 (21 kd) into the nucleus may occur by a facilitated mechanism which requires a cytoplasmic receptor. In general, the mechanisms of nucleocytoplasmic transport and its regulation are not known. However, active transport of large nuclear proteins (molecular weights >40 kD) requires specific nuclear localization signals (NLS) (Dingwall et al., 1982; Kalderon et al., 1984; Davey et al., 1985), is ATP dependent (Newmeyer et al; 1986*a* and *b*) and is inhibited by wheat germ agglutinin (WGA) (Finlay et al., 1987; Yoneda et al., 1987) and RL1, a monoclonal antibody specific for some O-linked *N*-acetyl glucosamine (GlcNAc) containing nucleoporins (Featherstone et al., 1988). Moreover, Dingwall and co-workers (1988) and Rihs and Peters (1989) have shown that sequences adjoining the minimal NLS of nucleoplasmin and SV40 large T-antigen are important for efficient nuclear localization in vivo.

Recent results suggest that the nuclear import pathway involves at least three steps: (*a*) rapid perinuclear accumulation of NLS containing proteins independent of temperature, (*b*) substrate binding to the NPC, and (*c*) translocation through the pore complex (Richardson et al., 1988; Newmeyer and Forbes, 1988). At the level of the pore complex, nuclear import has been resolved into distinct steps including (*a*) central docking of substrate to the

Dr. Akey's current address is Department of Biophysics, Boston University School of Medicine, 80 East Concord St., Boston, MA 02118-2394.

transporter which may be preceded by peripheral binding, and (*b*) an apparent gating event that is presumably coupled with translocation (Akey and Goldfarb, 1989). In addition, we have demonstrated that the central transport assembly within NPCs is specifically labeled with both WGA, a probe for GlcNAc containing nucleoporins and a potent transport inhibitor (Finlay et al., 1987), and mAb-414 a monoclonal which primarily recognizes np62 which is also glycosylated (Davis and Blobel, 1986). This suggests that the O-linked GlcNAc containing nucleoporins are intimately involved in transport at the level of the NPC transporter, possibly as receptors (but see Snow et al., 1987). Finlay and Forbes (1990) have recently shown that nuclei reconstituted from *Xenopus* oocyte extracts which have been depleted of the GlcNAc-containing nucleoporins are no longer competent for active transport of large proteins, although normal NPCs are assembled into the nuclear envelopes. Transport can be restored in this system by adding back WGA-affinity column fractions to the assembly mixture. Together these data strongly support the concept that the O-linked GlcNAc containing nucleoporins play a pivotal role in nucleocytoplasmic transport at the level of the NPC transporter. Furthermore, other soluble components may be involved in the regulation of transport and the formation of docked-substrate complexes, as demonstrated by the loss of specific nucleoplasmin-gold labeling of *Xenopus* NPC transporters when the reaction is carried out in vitro (Akey and Goldfarb, 1989). Indeed, Adams and coworkers (1989) have recently identified two proteins which specifically bind to an extended NLS of the SV40 large T-antigen. These putative NLS-binding proteins have been localized to the cytoplasm and nucleoplasm of cells, as well as to the nuclear envelope by cell fractionation experiments suggesting a role in nuclear import as carrier or receptor molecules.

A deciphering of the mechanism of NPC-mediated transport is central to understanding the pathway responsible for maintaining the compartmental distribution of proteins and RNPs in interphase cells: a distribution reestablished at the end of mitosis in eukaryotes undergoing open division. Recently, two nucleolar proteins that may facilitate nucleocytoplasmic transport of ribosomal components have been demonstrated to shuttle continuously between the nucleus and the cytoplasm (Borer et al., 1989): hence, shuttle proteins may represent a more general class of macromolecules involved in the regulation of nucleocytoplasmic transport and other nuclear activities. There is now mounting evidence to support the concept of developmentally-regulated nucleocytoplasmic localization of proteins (Dequin et al., 1984; Dreyer and Hausen, 1983; Servetnick and Wilt, 1987) and snRNPs (Zeller et al., 1983). Indeed, three groups have shown that nuclear localization of the dorsal morphogen (a transcription factor which is required for the developement of ventral structures in *Drosophila* embryos) is developmentally regulated (Rushlow et al; 1989; Steward, 1989; Roth et al., 1989). Furthermore, it appears that nuclear localization of this protein may be controlled by a regulated proteolysis of the cytoplasmically anchored complex (Rushlow et al., 1989; for review see Hunt, 1989). Nuclear export of mRNA transcripts may also be a spatially and temporally regulated process as nascent mRNAs have been shown to follow specific tracks from the nuclear interior to the periphery of the nucleus suggesting that the targeting of mRNPs to NPCs at the nuclear envelope may be involved in establishing cell polarity, morphology, and fate in development (Lawrence et al., 1989). Overall, these experiments reaffirm the pivotal role of the NPC as the gateway for transport and information exchange between the nuclear and cytoplasmic compartments of the cell (also see data reviewed by Dingwall and Laskey, 1986).

This report presents experimental observations which may be relevant to the gating mechanism of the NPC transporter. Specifically, the NPC transporter is visualized in frozen-hydrated nuclear envelopes in four possible transport-related configurations. The observation of apparent closed, docked, "in transit," and open forms in adjacent areas of the same images supports the hypothesis that nuclear import involves multiple steps at the level of the NPC transporter (Akey and Goldfarb, 1989). Furthermore, potential problems associated with the interpretation of images of the transporter labeled with nucleoplasmin-gold (Akey and Goldfarb, 1989) have been bypassed in this work. Finally, a working model of the NPC transporter and its role in nucleocytoplasmic transport are presented.

METHODS

Details of the preparation and computer alignment of a dataset of roughly 3,900 membrane-associated NPCs from *Necturus* oocyte nuclei have been described earlier (Akey, 1989*a*). In previous work the global projection averages of both detergent-extracted and membrane-associated NPCs were analyzed. This report focuses on the variable structure of the central transporter of membrane-associated NPCs and to that end the NPCs have been classified based on shared image features in this region. To a first approximation the NPC can be considered to consist of an outer framework which acts to support the central transporter (Akey, 1989*b*). Therefore, structural features between radii of 200–750 Å were addressed previously (Akey, 1989*a*). The analysis of interimage variance in electron micrographs and the implementation of classification methods has been pioneered by Frank and co-workers employing multivariate statistical analysis (van Heel and Frank, 1981), hierarchical ascendant classification (Frank et al., 1988), and a method of cluster determination based on the concept of fuzzy sets (Carazo et al, 1989). All three methods were used in combination in this work.

Individual aligned and scaled NPCs were eightfold averaged to enhance the signal of the transporter. The following analysis is depen-

dent on this step and indeed the real space alignment of NPCs is dominated by the eightfold symmetry of the spokes; hence, the central transporter is randomized in discrete angular multiples of 45 degrees in the unenforced dataset. Evidence from labeling studies with WGA-gold (Akey and Goldfarb, 1989; Scheer et al., 1988) and mAb-414 protein A-gold (Akey and Goldfarb, 1989), a probe which predominantly recognizes the nucleoporin p62 on western blots (Davis and Blobel, 1986; Finlay et al., 1987), suggests that the transporter may share the eightfold symmetry of the intact pore complex. Moreover, based on assembly considerations it seems unlikely that the transporter will have a symmetry which differs from that of the NPC. However, there are cases of symmetry mismatches in macromolecular assemblies: in particular, the construction of closed viral capsids of polyoma (Rayment et al., 1982) and SV-40 viruses (Baker et al., 1988) and in systems where two components have been postulated to rotate relative to each other, as exemplified by the phage connector-head mismatch (Hendrix, 1978). As shown herein, a viable model of transporter function can be constructed which does not require a solid body rotation of the transporter relative to the spoke assembly of the NPC. An experimental determination of the rotational symmetry of the NPC transporter should be feasible by labeling methods (Akey and Goldfarb, 1989), when monospecific probes are available for proteins within the central assembly.

The basic observations of this work are to some extent independent of the rotational symmetry assumed for the transporter. In all, 4,152 membrane-associated NPCs were subjected to correspondence analysis passing only the image pixels between radii of 0–200 Å. The data were then classified by hierarchical ascendant methods and fuzzy C means cluster analysis. The analysis produced four major image classes representing 30% or 1,251 particles and resulted in the discarding of 70% of the particles. This cut was not unexpected as the central transporter/plug is easily distorted or lost during specimen manipulations (Unwin and Milligan, 1982; Milligan, 1986; Akey, 1989*a*). Furthermore, during the initial particle selection from weakly defocused micrographs projected onto the AED monitor the central channel assemblies were basically invisible. Therefore, criteria for the selection of particles included the preservation of the strong eightfold symmetry of the spokes coupled with a circular particle profile and the absence of any obvious acentrically placed material in the region of the central transporter.

RESULTS

Initially, data are presented which demonstrate that the central transport assembly within NPCs can be observed directly in micrographs of nuclear envelopes without image processing. Subsequently, results of a classification analysis of 4,152 membrane-associated NPCs are presented which identify four possible transport-related forms of the NPC transporter. Constraints provided by the projection maps and the known physiology of the nuclear transport process are then used to construct a working model of the transporter and this hypothesis is presented in the discussion section.

Visualization of the NPC transporter

A micrograph of a spread nuclear envelope isolated from *Necturus* oocytes and imaged in the frozen-hydrated state is presented in Fig. 1. In this unstained and unfixed preparation the protein scatters more strongly than the intervening bulk lipid and amorphous ice and therefore is dark. Individual NPCs with eightfold symmetry are evident, and in favorable cases ringlike central transporters are visible within the NPCs (NPCs marked with black circles). In some instances the ringlike transporter appears to contain centrally located material (NPCs marked with white circles). A montage of selected NPCs demonstrating these features is presented in Fig. 2 *a* and the corresponding eightfold averaged NPCs are shown in Fig. 2 *b*, with protein dark as in the micrograph. In Fig. 2 *a*, central ringlike structures are evident in the first 13 particles between radii of 0–200 Å. The NPCs in the first row appear to have a more restricted central pore than those in the second row, as seen more clearly in the corresponding images in Fig. 2 *b*. The NPCs in rows 3 and 4 (excluding the first and last) were chosen to demonstrate ringlike transporters with an associated central density which may correspond to endogenous substrates caught in transit during isolation (also see images in Fig. 2 *b*). This supposition seems reasonable given that mRNPs can be visualized in transit through NPCs in fixed and sectioned material (Stevens and Swift, 1966; Franke, 1974; Mehlin et al., 1988). Average projection maps of nucleoplasmin-gold labeled NPCs obtained by manual classification demonstrated a similar phenomenon with some gold particles apparently having been caught in transit (Akey and Goldfarb, 1989). Moreover, central ringlike features between radii of 0–200 Å have been observed previously in frozen-hydrated specimens of detergent-extracted NPCs (Akey, 1989*a*) and are selectively labeled with colloidal gold probes containing bound WGA, nucleoplasmin or mAb-414 (Akey and Goldfarb, 1989).

Averages from 50 NPCs in Fig. 1 are shown in the bottom right panels of Fig. 2 *a* and *b*. The average projection in Fig. 2 *a* has not been eightfold averaged and although noisier compares favorably with its eightfold averaged counterpart in Fig. 2 *b*, indicating the general quality of the data. A central ringlike transporter is present in both maps. The radial arm features observed previously (Akey, 1989*a*; also see Figs. 3 and 4 *a*) are present in most of the individual eightfold averaged NPCs and possess approximate mirror symmetry in the averages. In projection, the observed mirror symmetry implies that the features of the NPC which give rise to the radial arms are present in both of the nearly equivalent halves of the NPC related by a twofold axis oriented parallel to the nuclear envelope and perpendicular to the central eightfold axis. These data are in agreement with previous observations that the detergent-extracted NPC has approximate 822 symmetry at 65 Å resolution (Akey, 1989*a*; Milligan, 1986). The radial arms are comparable in intensity to the central transporters in individual

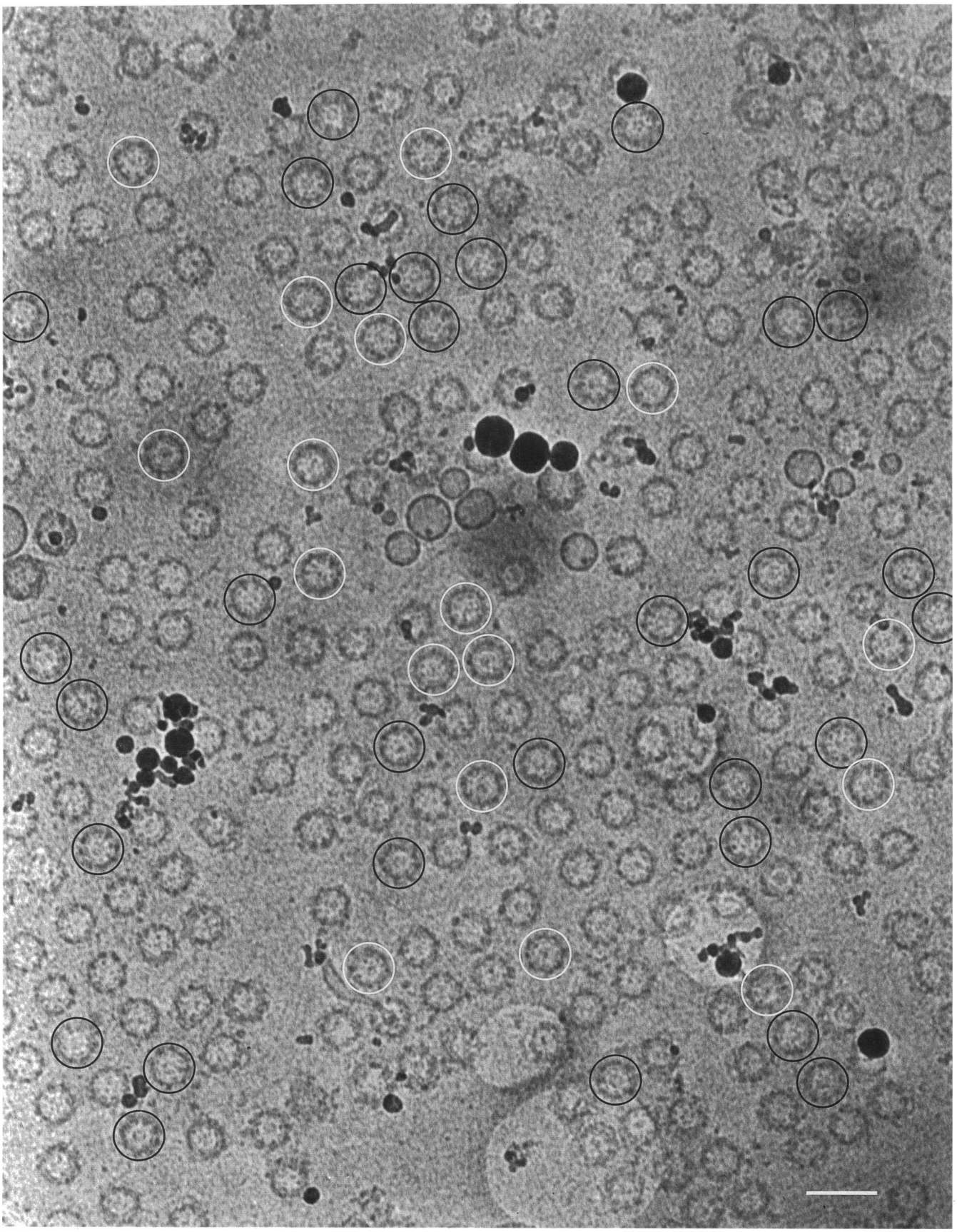

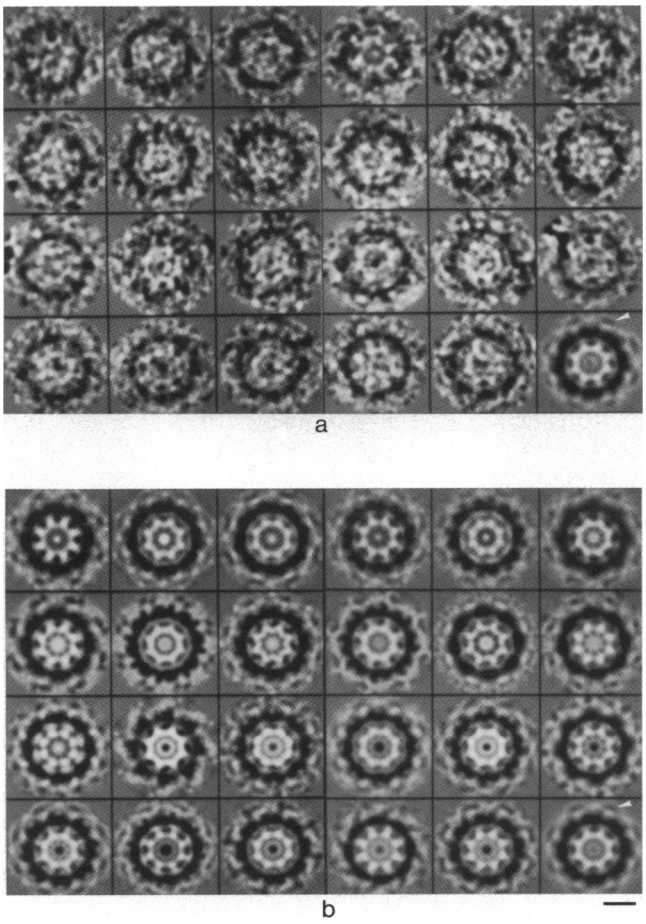

FIGURE 2 (*a*) A montage of 23 aligned NPCs selected from the micrograph in Fig. 1 is presented. The NPCs in the top two rows have ringlike central transporters, whereas those in the last two rows (excluding the first and last particles) appear to have material caught in transit. The last bottom right panel shows a global average of ~50 NPCs from this micrograph, without symmetry enforcement during the processing. Note the presence of the central ringlike channel. (*b*) A montage is shown of the corresponding eightfold averaged NPCs from *a*. Note that the individual NPCs show both ringlike central transporters and well defined radial arms at their peripheries. A global average in the bottom right panel shows these features and should be compared with its counterpart in *a*. Protein is in the same contrast as Fig. 1 and is black. The diameter of the globally averaged NPC is ~1,450 Å including the radial arms, marked with a white arow. Scale bar, 500 Å.

NPCs; however, the central transporter is weaker in global averages presumably as the result of including NPCs in the averages with lost, disordered or variable transporters (see Akey, 1989*a*). A precise role for the radial arms has not been elucidated although it has been posulated that they may be involved in anchoring the pore complex to the nuclear envelope (Akey, 1989*a*).

Projection maps of the transporter

A dataset of 4,152 membrane-associated NPCs was sorted into classes containing images with common transporter features using computer-based methods (Frank et al., 1988; Carazo et al., 1989), resulting in four major classes containing a total of 1,251 NPCs. These transporter classes have been tentatively identified as closed, docked, "in transit," and open forms (but see below). Individual classes were then divided randomly into half datasets to check the internal consistency and resolution of the class averages. As an example, two half-dataset averages of the "in transit" form of the NPC are presented in Fig. 3 *a* and *b* in reverse contrast with protein white. The features of the membrane-associated pore complexes in these maps are consistent with projection maps of selected averages shown previously (see Fig. 3 legend and Akey, 1989*a*), though more symmetric. Features of the central ringlike transporter are conserved between the two half-datasets of this class. Note that the apparent "subunits" of the transporter are rotationally offset from the spoke assembly by 22.5 degrees in a staggered configuration. The half-dataset averages in Fig. 3 possess reliable information to a resolution of ~60–65 Å as determined by Fourier ring correlation (van Heel, 1987); half-datasets of the other major classes were of comparable quality.

Further details of the "in transit" form are presented in Fig. 4. The final class average from 342 NPCs is shown in Fig. 4 *a*, while a map at a higher cutoff which emphasizes the apparent symmetry of the stronger features is shown in Fig. 4 *b*. The rotationally equivalent unit in point group C8 is indicated by the intersecting arrows which also correspond to apparent mirror lines in projection, creating a second line of mirror symmetry at 22.5 degrees between them (not shown). In panel *c* a variance map for the average projection is shown with variance hot spots in black. There are four major peaks (labeled 1–4) with the highest peak lying on the eightfold axis. This peak presumably represents the variability (along the direction of view) of substrates caught in transit. Peaks 2 and 4 occur over the vertical supports/rings (VS) and at the junction of the inner and outer spokes with the nuclear envelope border. These two peaks represent the previously noted sites of variability of membrane-associated NPCs (Akey, 1989*a*) and may result from specimen deforma-

FIGURE 1 Electron micrograph of a spread nuclear envelope from a *Necturus* oocyte, prepared and imaged in the frozen-hydrated state. Protein is dark. Individual NPCs display eightfold symmetry and those encircled in black demonstrate a ringlike central transporter, while those encircled in white appear to have been caught with endogenous material in transit. See Fig. 2 for selected particles. Scale bar, 2,000 Å.

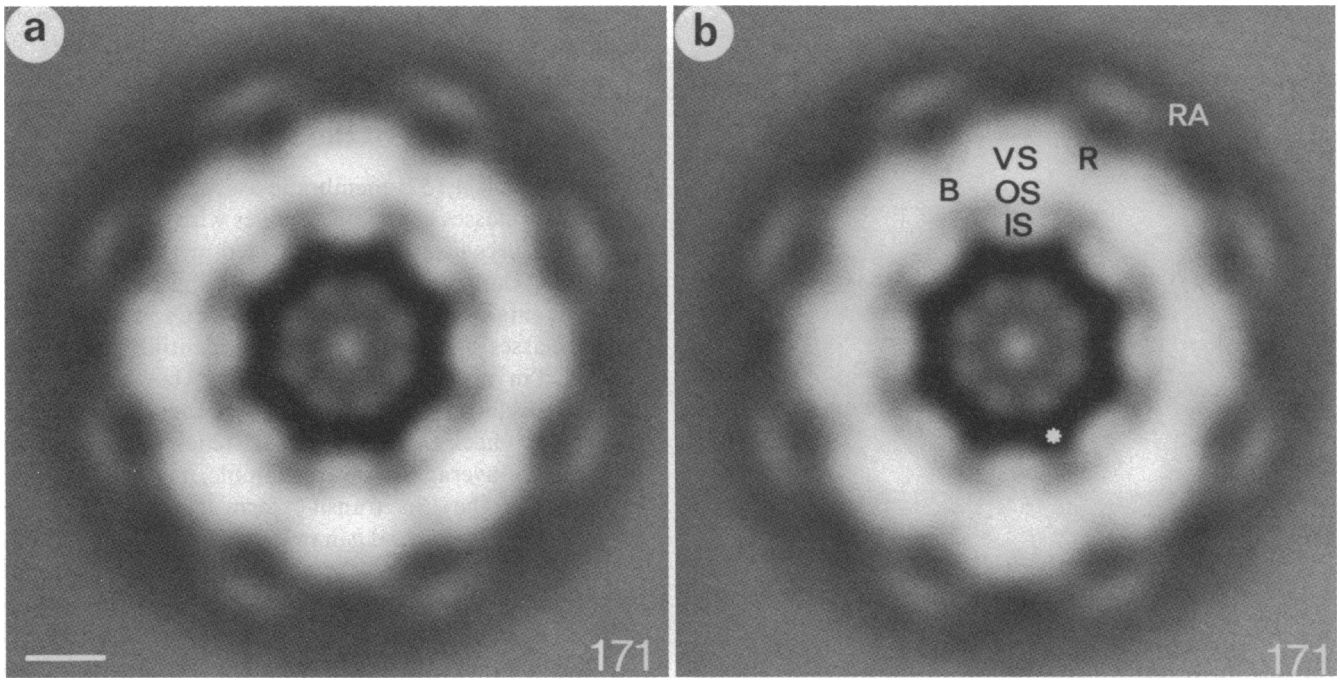

FIGURE 3 Average projection maps are presented of half-datasets of the "in transit" form of the NPC (171 particles in each). Protein is white in these and subsequent maps. Features of the maps include the radial arms (*RA*) which exhibit good mirror symmetry, the membrane boundary (*B*), and three domains of the spoke assembly including the inner spokes (*IS*), outer spokes (*OS*), and vertical support region (*VS*), which arises from a superposition of the coaxial rings and their vertical supports (see Akey, 1989*a*). The central transporter is composed of eight peripheral density peaks which surround a central peak and a dark ring which may represent the edge of the expanded transport pore. Not shown at this cutoff are reproducible weak cross-bridges which link the transporter to the ends of the spoke assembly. The white asterisk indicates one of eight apparent peripheral channels of ~50 Å diameter which may be involved in passive transport. Scale bar, 200 Å.

tions during manual isolation as the result of swelling of the perinuclear space. A more detailed analysis of this phenomenon is in progress. The high degree of 822 symmetry observed in these maps is interesting as this feature was not selected for in the classification analysis. In general, averages of the 22 projection datasets analyzed previously (Akey, 1989*a*) ranged from strongly asymmetric (NPCs from *Xenopus*) to more nearly symmetric. Detergent-extracted NPCs from *Necturus* (which are attached to the nuclear lamina) demonstrate marked 822 symmetry (Akey, 1989*a*), in agreement with projection maps from detergent-extracted and detached *Xenopus* NPCs (Unwin and Milligan, 1982; Milligan, 1986). In contrast, detached spoke assemblies which have apparently lost their thin rings are markedly asymmetric, even in the inner spoke regions (Reichelt et al., 1990). Although the NPC is vectorial in its transport properties (Dingwall and Laskey, 1986), it is not yet clear whether this property is manifested in the low-resolution structure of the NPC. However, the NPC must be asymmetric with regard to side-specific associations of which attachments to the nuclear lamina (Aebi et al., 1986) and possible cytoplasmic granules (Unwin and Milligan, 1982) are examples.

A gallery of four class averages of the NPC transporter is presented in Fig. 5. Only the central transporters and a small region of the adjoining spoke assembly are shown in these maps.

(*a*) *Closed form.* In Fig. 5 *a*, the average transporter (labeled *T*; $n = 343$) is weakly modulated with an apparent central pore of 90–100 Å diameter and is less stellate than a previous average from a smaller number of NPCs (Akey, 1989*b*). This class may represent a closed configuration of the transporter as Paine and co-workers (1975) have shown that the limiting diameter of the passive diffusion pore in *Xenopus* oocytes is ~90 Å.

(*b*) *Docked form.* The class in Fig. 5 *b* ($n = 314$) is characterized by a more stellate appearance of the transporter (labeled *T*) and the presence of material apparently docked over the central pore. This map agrees remarkably well with projection maps of transporters with centrally-docked nucleoplasmin-gold particles from a much smaller dataset (Akey and Goldfarb, 1989). The points of the eight-sided star are aligned slightly askew

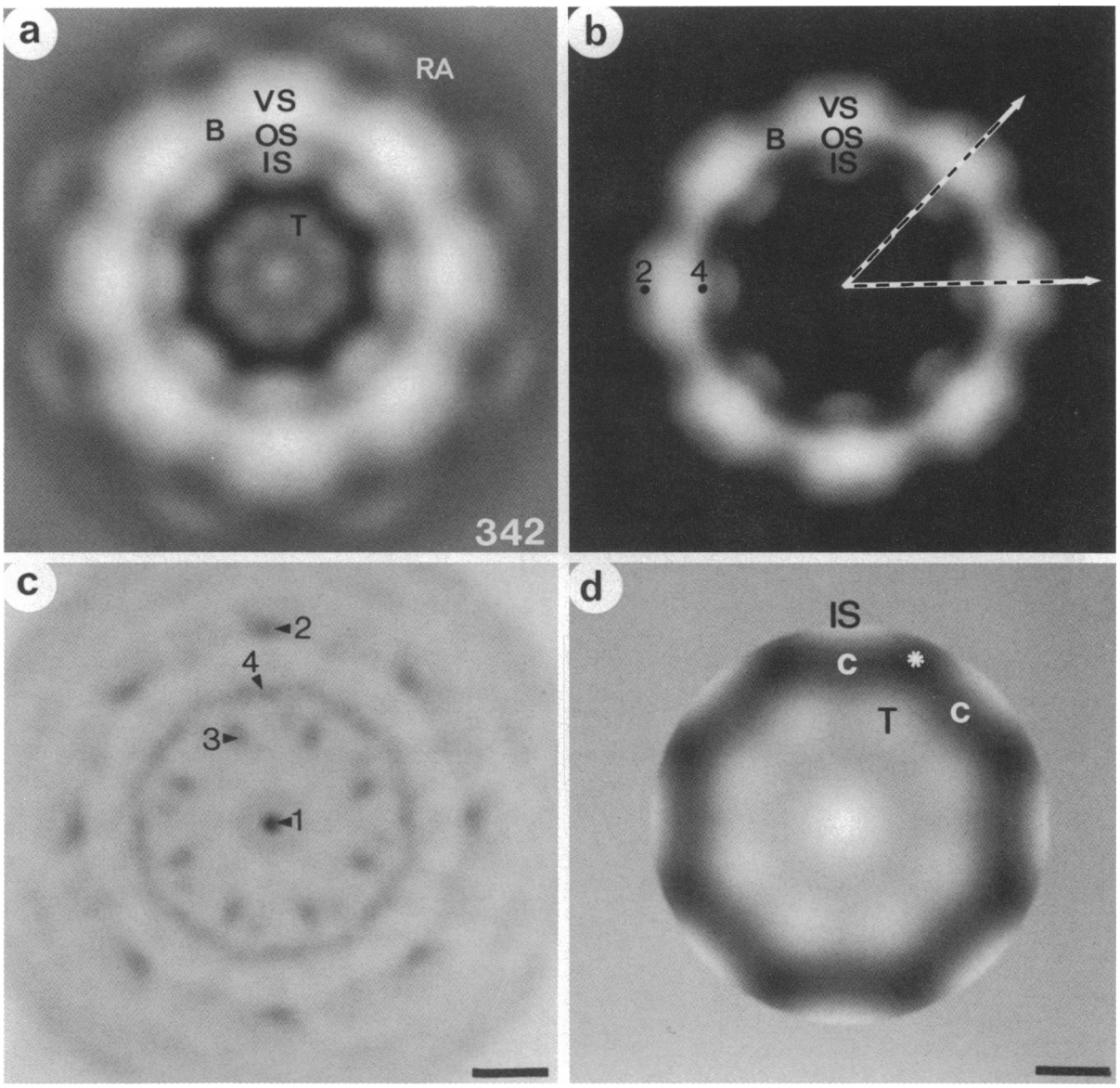

FIGURE 4 An in-depth characterization of the "in transit" form: (*a*) Total class average with $n = 342$. Features are labeled as in Fig. 3. Note the apparent 822 symmetry of the complex. (*b*) The same map as in panel *a* is shown at a higher cutoff to emphasize the marked mirror symmetry of the strongest features. A single rotationally equivalent unit in C8 is indicated by the intersecting dashed arrows, which also correspond to approximate lines of mirror symmetry. Radial positions of some of the larger variance peaks are indicated (*black dots 2 and 4*). (*c*) Variance map for panel *a*. Four major peaks are present including a ring of weak density at position 4. Scale bar for *a–c*, 200 Å. (*d*) Enlarged cutout of the central transporter assembly shown at a lower cutoff than in *a*. Note the eight peripheral pores (*white asterisk*) formed by the weak connections (*c*) between the inner spokes (*IS*) and the transporter ring (*T*). Scale bar, 100 Å.

from a staggered orientation with respect to the spoke assembly. The central density over the transporter appears somewhat diffuse implying that a portion of the putative transport substrates may be docked slightly off axis in individual NPCs. Similarly, nucleoplasmin (an endogenous substrate in oocytes) has been shown to bind to the transporter both centrally and peripherally by quantitative analysis of nucleoplasmin-gold labeling (Akey and Goldfarb, 1989). A mixture of peripherally and centrally attached substrates would generate the diffuse density observed over the transporter after eightfold averaging.

(*c*) *In transit form.* In Fig. 5 *c* the average transporter ($n = 342$) consists of a ring of eight density peaks and

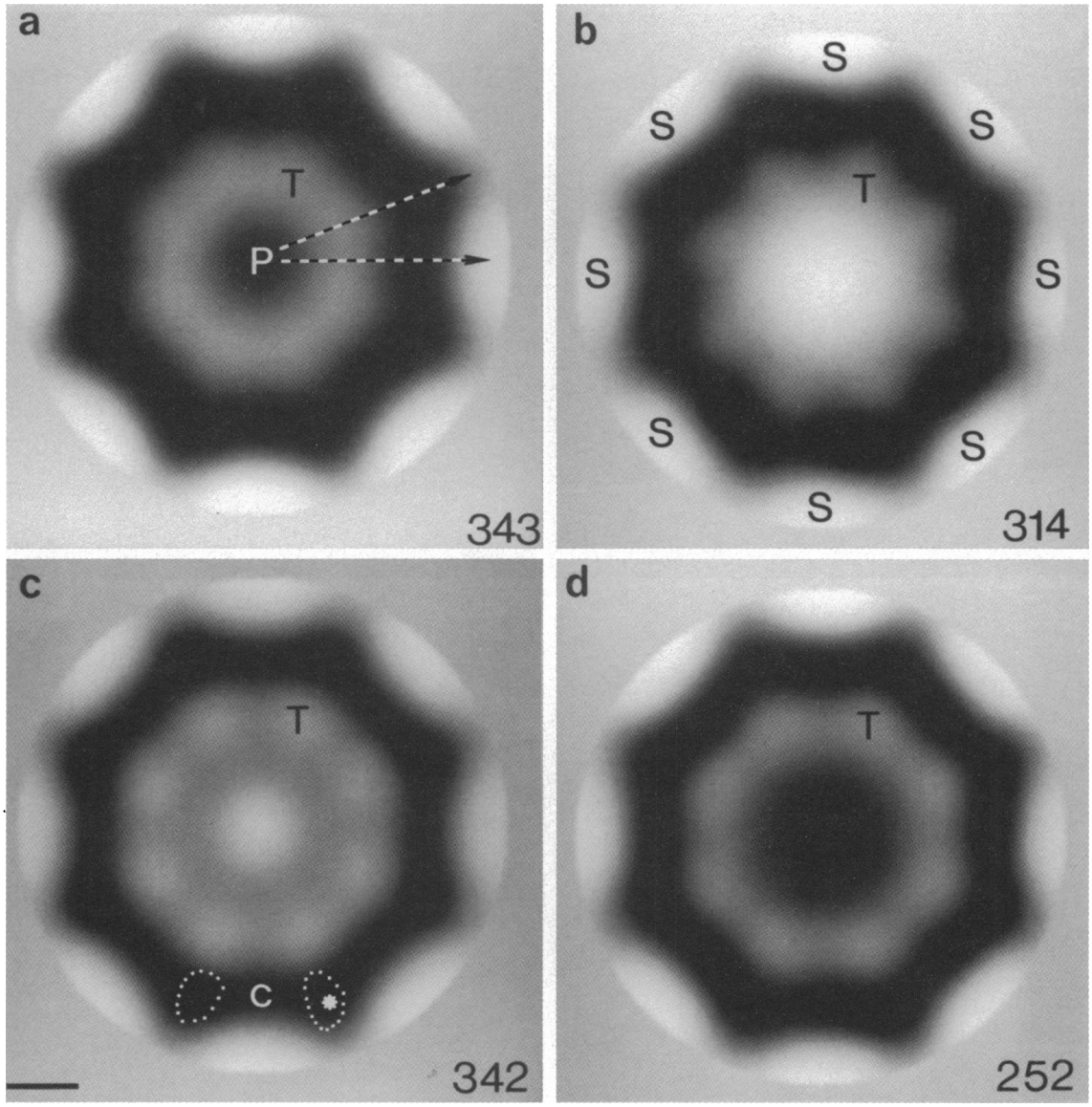

FIGURE 5 Average projection maps of four classes of central transporters in the staggered orientation are shown. Protein is white and only the central region of the NPCs is presented. Transporter subunits are labeled *T* and the peripheral ends of the spokes are labeled *S*. (*a*) An average of 343 particles of the closed form is presented. The apparent central pore (*P*) is ~90 Å in diameter. The two independent twofold axes in point group 822 are shown. (*b*) An average of 314 NPCs with docked central transporters is presented. The transporter has a stellate appearance and is slightly skew from the local twofold axes shown in panel *a*. (*c*) An average of 342 "in transit" forms is shown. The white asterisk marks one of eight potential peripheral channels which may be involved in passive transport. At a lower cutoff (see Fig. 4 *d*), the region labeled *C* and bordered by white dots which delineate adjacent low density holes, may represent connecting density which presumably mediates attachment of the transporter to the spokes. (*d*) A map of 252 transporters in the average open form is presented. The transporter in this configuration shows an annulus of eight densities at a radius of 140 Å. The transporter appears to have a diameter of 360 Å in projection excluding the connectors. Scale bar, 100 Å.

appears expanded about a central density which may correspond to substrates caught in transit during nuclear isolation. The general appearance of this class agrees favorably with a smaller dataset of nucleoplasmin-gold labeled *Xenopus* NPCs (Akey and Goldfarb, 1989). In addition, the frequency of occurrence of the "in transit" form relative to the other classes appears too high to be the result of random trapping of material in the open transporter during isolation although this possibility cannot be totally excluded (but see below).

(*d*) *Average open form.* In Fig. 5 *d*, the central transporter ($n = 252$) appears open in projection based on the

size of the pore which measures ~180 Å in diameter. The open transporter in this map is rather similar to the "in transit" form in Fig. 5 *c*. The presence of the open form in cells would abrogate the transport selectivity of nuclei. Hence, the open form may originate during isolation by the loss of central substrates from "in transit" forms, resulting in a rigorlike open state in the absence of ATP or other protein co-factors in the isolation buffer. The size of the central channel in the putative open and "in transit" forms is comparable (180–200 Å diameter) suggesting a possible relationship between them.

(*e*) *Common features and minor classes.* A global average of the entire dataset of aligned transporters (n = 4,152) is shown in Fig. 6 *a*. For comparison a group average of the four major classes is shown in Fig. 6 *b*. Major features of the class averages like the annulus of eight densities (labeled *T*) and the central density, which may correspond to trapped substrates, are common to the global average in Fig. 6 *a*, though the features are more blurred and have altered intensities. This is a good indication that the major image classes which contribute to the global transporter average have been identified. All four class averages in Fig. 5 have a roughly staggered alignment with respect to the spokes and apart from the docked form, demonstrate an approximate twofold symmetry, apparent as eight lines of mirror symmetry spaced 22.5 degrees apart round a circle whose origin is the center of the map (see Fig. 5 *a* for the position of two unique twofold axes). Moreover, the data are consistent with observations that detergent-extracted NPCs are constructed with approximate 822 symmetry at 65 Å resolution (Akey, 1989*a*; Milligan, 1986). The mirror symmetry present in the maps has not been introduced spuriously during image processing as the handedness displayed by subaverages of membrane-associated NPCs in the dataset allowed an unambiguous determination of their up and down orientations (Akey, 1989*a*). Furthermore, these determinations had a strong correlation with the probable orientation of the specimens in the microscope during data collection. At a lower density threshold (see Fig. 4 *d* for "in transit" class), each class also demonstrated weak connections between the transporter "subunits" and the inner spokes in the region labeled *c* in Fig. 5 *c*. These connections were present in 22 individual averages of the dataset (Akey, 1989*a*) and result in the demarcation of eight peripheral regions of low density of ~50 Å diameter, located between the transporter and the spoke assembly (labeled with white asterisks in Figs. 3 *b* and 4 *d* and shown as white dotted features in Fig. 5 *c*). These peripheral regions may correspond to pores with diameters smaller than the measured passive diffusion limit of 90 Å (Paine et al., 1975). Interestingly, peak 3 in the variance map (Fig. 4 *c*) aligns with the peripheral pores. The reason for this degree of variability is not clear, especially as this region is the strongest negative density feature in the map. However, the variance is low over the weak connecting bridges adjacent to the peripheral channels. A proper three-dimensional map is needed to address these observations.

Finally, two minor classes were identified by the classification analysis which appear to have transporters in an aligned and slightly skew orientation with respect to the spoke assembly. Moreover, at lower density cutoffs the projection maps (data not shown) also show the eight connecting densities and the putative peripheral pores observed in the staggered forms. These two classes represent an additional 4% (n = 245) of the total dataset and 16% of the classified images. A fraction of aligned transporters (~33%) was observed previously in a small sample of *Xenopus* oocyte NPCs labeled with nucleoplasmin-gold (Akey and Goldfarb, 1989). The functional significance of the aligned form remains to be determined; however, it may represent residual noise or an alternate packing of the transporter within the NPC (Akey and Goldfarb, 1989).

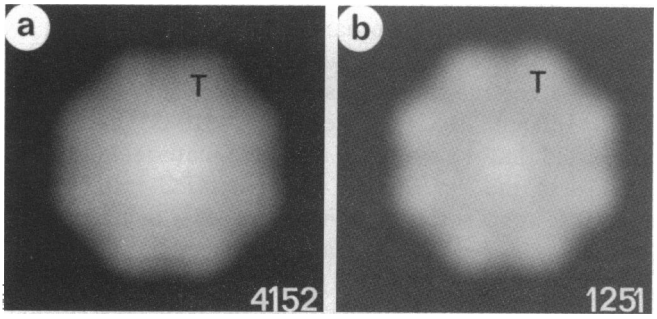

FIGURE 6 Global projection maps of the transporter: (*a*) The entire dataset (n = 4,152) of membrane-associated NPCs, (*T*) transporter annulus. (*b*) Group average of the four major classes (n = 1,251). Note that the features of the average are also present in panel *a*.

DISCUSSION

The preparative and computational methods used in this work have been shown to be reliable, as demonstrated by the reproducibility of separate averages of detergent-extracted NPCs (Akey, 1989*a*) and the agreement shown herein between half-datasets of the four major classes. In fact, the radial arm features exemplify the ability of single particle alignment methods to reproducibly extract weak details not visible by eye from low-dose images (Frank et al., 1981). As in crystallographic analysis where spatial averages are obtained from repeating motifs in a crystal, single particle methods extract a spatial average of image features common to individual particles

which have been computationally aligned. The efficacy of the single particle method in retrieving information is determined by the accuracy of the computer-based alignments, which in turn are dependent on specimen preservation, the signal present in low-dose micrographs, and the adoption of unique specimen orientations with respect to the electron beam. In this respect the nuclear envelope is a favorable specimen as NPCs possess eightfold rotational symmetry and are constrained by interactions with the nuclear envelope and lamina to be roughly co-planar (Akey, 1989*a*), thereby allowing correction of in-plane translational and rotational disorder by cross-correlation alignment methods (Frank et al., 1981).

Multiple forms of the transporter

The results of this study suggest that NPCs in unfixed nuclei prepared by manual isolation and rapid freezing for cryoelectron microscopy, contain central transporters in a minimum of four related configurations. Preparation of nuclear envelopes in the frozen-hydrated state is crucial as the transporter and the NPC appear to be readily damaged by conventional preparative methods. Pore complexes in *Xenopus* oocytes are known to be transport competent (Feldherr et al., 1984) and the translocation mechanism is energy dependent (Newmeyer et al., 1986*a*, *b*). Although little is known about the mechanism of transport, the process is likely to be cooperative as the transporter is capable of transporting substrate-coated gold particles with diameters of up to 260 Å (Dworetzky and Feldherr, 1988) while maintaining a passive diffusion pore of ~90 Å (Paine et al., 1975). This represents an ability to regulate the central transport pore over a range of effective diameters of 90–260 Å! Hence, it does not seem unreasonable that the NPC transporters in nuclei would be trapped in a range of transport-related states during rapid isolation from living oocytes into buffers lacking co-factors. Therefore, the different classes of transporters observed in this study may represent forms which are relevant to nucleocytoplasmic transport. The visualization of ringlike transporters probably does not result from degradative processes as detergent-extracted *Xenopus* NPCs prepared rapidly in buffers with protease inhibitors also demonstrate different transporter configurations (data not shown). Artifacts arising from averaging membrane-associated NPCs in various stages of disassembly would seem to be ruled out by the observation that the class averages of membrane-associated NPCs demonstrate a more marked 822 symmetry than earlier averages (see Fig. 4 and Akey, 1989*a*), suggesting that they are well preserved. However, a direct physiological interrelationship between the different observed forms has not yet been demonstrated.

A number of salient features of the NPC transporter have emerged from these studies. First, the apparently closed form has a central pore of ~90–100 Å diameter in agreement with the limiting pore size in *Xenopus* oocytes determined for passive diffusion (Paine et al., 1975). Second, there are weak features which appear to connect the transporter and the inner spoke domains within NPCs, resulting in the demarcation of eight apparent peripheral pores of ~50 Å diameter. Third, transporters with either nucleoplasmin-gold (Akey and Goldfarb, 1989) or endogenous material bound in a docked configuration appear to have a stellate appearance in projection. The stellate shape is also present in a small dataset of closed NPC transporters reported previously (Akey, 1989*b*). It is possible that the closed transporters in this study have the stellate shape but are somewhat disordered whereas the docked form is stabilized by bound substrate. Alternatively, a small rearrangement may occur upon formation of the docked complex. In fact, the docked and "in transit" forms appear to be comparable to their counterparts observed in a study of the interaction of nucleoplasmin-gold with *Xenopus* NPCs after microinjection (Akey and Goldfarb, 1989). I would stress that the open form observed in this work probably does not represent a physiological intermediate in transport with an appreciable lifetime as it would result in a loss of selectivity. Instead, this class may arise by the fortuitous loss of substrates from "in transit" forms during specimen preparation. Consistent with this hypothesis the major features of transporters in this class are similar to those displayed by the "in transit" class. The transporters in both classes are comprised of an annulus of eight peripheral densities and exhibit additional mirror symmetry in projection, implying that the transporter is constructed along lines consistent with the approximate 822 symmetry of the pore complex (Milligan, 1986, Akey, 1989*a*). The observed 822 symmetry suggests that the transporter at this resolution is composed of two equivalent or nearly equivalent halves each of which possesses eightfold symmetry; hence, there must be at least 16 "subunits" involved in the gating mechanism of the transporter.

Previous architectural models of the NPC have described a central plug or granule (Franke, 1974; Unwin and Milligan, 1982; Scheer et al., 1988) and have suggested that the plug may represent material in transit. Details of the "in transit" class of NPC transporters appear to support this hypothesis. It is easy to understand how en face views of the transporter assembly could be described as a plug given the positive staining of in-transit mRNPs in sectioned material and the poor preservation of most negatively stained specimens coupled with the lack of statistically defined averages. Furthermore, the plug was measured to be roughly 300–350 Å in diameter consistent with dimensions of the average "in transit" complex of the transporter in this work. Additional

evidence from work on visualizing mRNPs in transit (Stevens and Swift, 1966; Franke, 1974; Mehlin et al., 1988), suggests that mRNPs form an unusual class of transport substrates in which the larger complexs must unroll before transport through the center of the NPC. The apparent diameter of these mRNPs in transit is ~150–200 Å, a value smaller than the observed dimensions of the plug but consistent with the known transport capability of the NPC transporter (Dworetzky and Feldherr, 1988) and the dimensions of the average open form described in this work.

Hypothesis: a model of the NPC transporter

The NPC transporter is unprecedented in its ability to transport both large globular macromoleucles (for a review see Dingwall and Laskey, 1986) and large mRNPs in an unrolled and extended configuration (Stevens and Swift, 1966). In addition, the NPC is capable of bidirectional transport (Dworetzky and Feldherr, 1988). What type of transport mechanism is capable of this diversity while maintaining the required specificity? To date, no model has been proposed which can adequately explain the known characteristics of nucleocytoplasmic transport. However, projection maps of the NPC transporter place constraints on the types of transport models which can be constructed when combined with data on the physiology of the transport process. An initial working model of the transporter is presented in Fig. 7 *a* and consists of two rings of subunits related by an approximate twofold axis, with each ring having an irislike arrangement. Individual subunits would be comprised, in part, of a mechano-ATPase which can rotate about its distal end through an angle of ~20–25 degrees in a concerted fashion to generate an irislike dilation of the transporter (see Fig. 7 *b*). Notably, nuclear envelope–associated ATPases have been described but not yet purified (Berrios and Fisher, 1986; Baglia and Maul, 1983). Furthermore, the "subunits" in adjacent irises probably are not in physical contact over an extensive area. Instead, the two layers may be puckered when viewed in cross-section maintaining interlayer contacts only at outer radii to minimize mechanical resistance to the radial sliding motions of the subunits as they iris open. Interestingly, the length of the putative mechano-ATP-ase subunit in the model approximates the size of the ordered portion of the myosin S_1 head (Milligan and Flicker, 1987).

The central pore in Fig. 7 *a* is 90 Å in diameter in the closed form while the fully dilated form has an expanded pore of 210 Å (Fig. 7 *b*). Models which encompass larger dilations can be constructed by changing the shapes and packing of the iris "subunits." An irislike arrangement

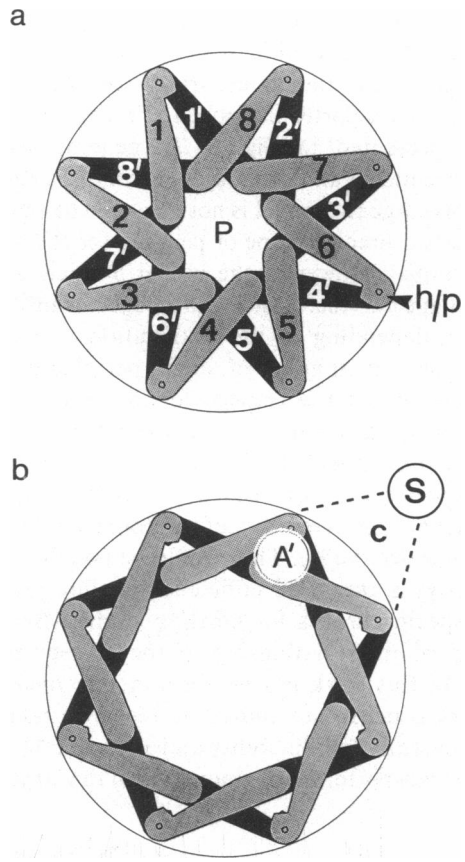

FIGURE 7 Diagram of the double iris model of the NPC transporter: (*a*) The closed form is shown viewed normal to the plane of the nuclear envelope. The model consists of two layers each of which is comprised of eight subunits which together form a supramolecular double iris. The layers are related by a twofold axes of symmetry and the subunits in the assembly conform to 822 symmetry, although the structure will probably deviate from strict 822 symmetry at higher resolution and at select times during the transport cycle. The individual subunits in each layer are numbered. In addition, the central pore (*P*) and putative hinge regions (*h/p*) are marked. The overall diameter of the transporter, excluding connections to the spokes, is ~360 Å. The exact alignment of the "subunits" and the true hand of the irises is not known. (*b*) The open form of the transporter model is shown. The individual subunits have rotated ~20–25 degrees about their distal ends resulting in the juxtaposition of portions of four different "subunits" as indicated (*A'*). The central expanded pore is ~210 Å in diameter and the relative position of one of the spokes is indicated (*S*).

appears to represent an optimal way to construct a supramolecular assembly capable of large dilations while minimizing the physical size of the iris "subunits" and the angle through which each "subunit" must move during gating. Alternative swinging or sliding "double door" models appear implausible based on mechanistic and steric grounds. A swinging door model would not generate a symmetrical "in transit" complex while a sliding door

model would seem incompatible with the types of motions displayed by known mechano-ATPases.

A comparison of the double-iris model with projection maps of the transporter in docked, "in transit" and open forms is presented in Fig. 8. In general, agreement between the model and the projection maps is encouraging. At this stage the model is not meant to be space filling or to dictate a precise shape or packing for the individual iris "subunits." However, the model predicts a roughly stellate shape for the closed and docked transporters in projection, depending on the distribution of mass in the subunits and an annulus of eight peripheral densities around the rim of the transporter in the open and "in transit" forms. As noted previously there are two caveats to the proposed model. First, the rotational symmetry of the transporter has not been determined unequivocally independent of the symmetry of the pore complex (but see discussion in Methods). This should be possible when the biochemistry is unraveled sufficiently to allow preparation of monospecific probes for labeling studies. Second, the physiological interrelationship of the transporter forms observed in this work has not been determined. Clearly more work is needed to address this central point. However, the overall reproducibility and apparent 822 symmetry of the transporter maps coupled with the large number of NPCs in the class averages suggests that the observations on which the model is based are reliable. In addition, ringlike central transporters have been observed in detergent-extracted NPCs (Akey, 1989*a*; and unpublished data from *Xenopus*) and can be labeled in ringlike patterns by nucleoplasmin (a transport substrate), WGA (a transport inhibitor), and mAb-414 which recognizes O-linked GlcNAc containing nucleoporins (Akey and Goldfarb, 1989).

The concept of a double irislike assembly appears to explain many properties of nucleocytoplasmic transport and immediately suggests a cross-linking mechanism of transport inhibition for WGA (Finlay et al., 1987; Yoneda et al., 1987) and RL1 (Featherstone et al., 1988). A WGA binding site has been mapped between radii of 100–125 Å on the transporter (Akey and Goldfarb, 1989). The WGA dimer has dimensions of 40 × 40 × 70 Å and possesses four potential carbohydrate binding sites, with the outer one in each subunit appearing to bind preferentially to substrates (Wright, 1977). The WGA dimer is therefore capable of acting like a small antibody and given the dimensions of the transporter model (~360 Å diameter) could cross-link adjacent "subunits" in a given iris, thereby preventing dilation. Furthermore, the monoclonal RL1 has been demonstrated to inhibit both

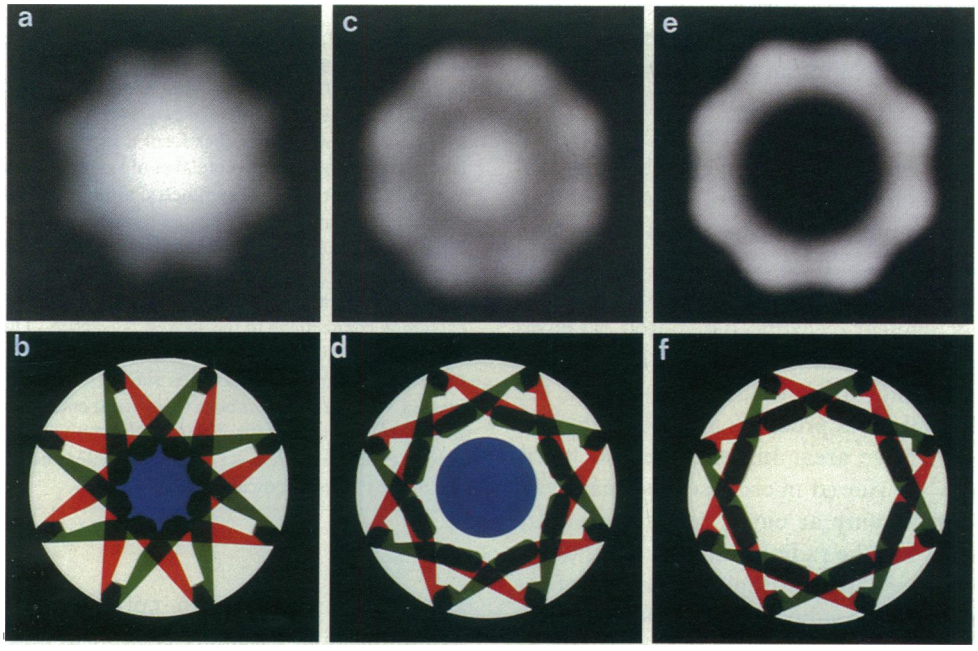

FIGURE 8 A comparison of selected projection maps of the NPC transporter in different transport-related configurations with corresponding simulated projections using a colored perspex model of the double iris. (*a* and *b*) The docked form; (*c* and *d*) the "in transit" form; (*e* and *f*) the open form. The annulus of eight strong peripheral densities in the open and "in transit" forms is generated by the juxtaposition of four different subunits of the double iris near the hinge regions.

nuclear import and export after microinjection (Featherstone et al., 1988) and has a specificity similar to mAb-414 for the O-linked GlcNAc containing nucleoporins. The binding site of the latter has been mapped on the transporter between 100 and 125 Å (Akey and Goldfarb, 1989). Given the flexibility of the carbohydrate containing epitopes and the size of the mAbs, RL1 could cross-link adjacent "subunits" as suggested by Featherstone and co-workers (1988) to prevent dilation. Moreover, the inhibition of active transport by RL1 or WGA does not block the passive diffusion of small macromolecules (Featherstone et al., 1988; Finlay et al., 1987; Dabauvalle et al., 1988). In the double-iris model WGA or RL1 could cross-link adjacent "subunits" without blocking the central 90 Å passive diffusion pore or the peripheral pores.

The model further suggests that the transporter may be involved in maintaining transport specifity. A double irislike assembly would maintain transport fidelity by functioning like a set of "macromolecular locks" with individual irises opening asynchronously relative to each other during the transport cycle (see Fig. 9 for details). The model is intrinsically bidirectional; hence, the transport mechanism of both nuclear import and export are predicted to share similar properties at the level of the transporter (see Dworetzky and Feldherr, 1988; Featherstone et al., 1988). Can the double-iris model explain, at least qualitatively, how elongated mRNPs can be translocated through the center of the transporter? The export of an elongated substrate may follow a path similar to that of globular substrates; however, in order for an mRNP particle to move through the expanded pore it may be necessary to alternately release and contract opposing irises in a cyclical manner, thereby forcing the extended mRNP particle through the expanded pore. Alternatively, one could envisage an extended mRNP particle being pulled through the NPC along linear tracks by a mechano-ATPase in a railroad type mechanism. However, there is little evidence to support this possibility and the data reported herein would argue against continuous fibers traversing the NPC. Instead, it seems likely that the mechanisms for the transport of globular and extended substrates will have some features in common.

Finally, if the principle of the double-iris model is correct, a determination of the 3D structure of the NPC transporter and characterization of the control mecha-

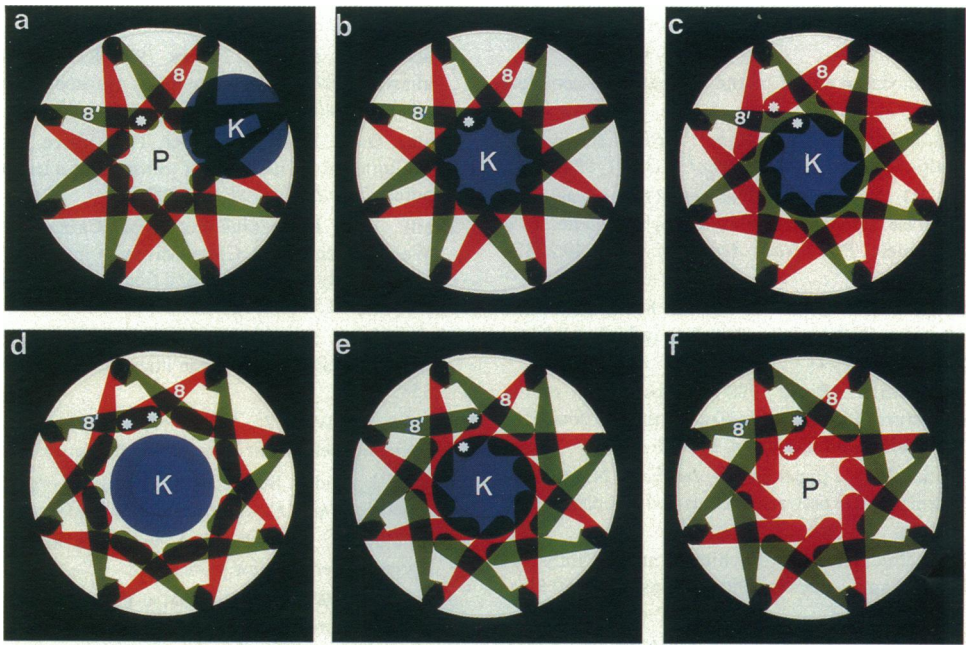

FIGURE 9 Hypothetical nuclear import sequence with a blue disk as karyophilic substrate (*K*). The asynchronous nature of this hypothetical transport cycle is evident from following points (defined by asterisks) on two symmetry-related subunits of the double irislike assembly. (*a*) Substrate binds peripherally to the transporter; (*b*) substrate docks over the central transport pore (*P*); (*c*) top (red) iris opens to admit substrate; (*d*) bottom (green) iris opens as substrate moves further into the transporter creating a symmetrical "in transit" form; (*e*) top (red) iris closes behind the substrate as it moves further into the expanded pore; (*f*) substrate dissociates from the inner surface of the NPC transporter. The bottom (green) iris then closes in preparation for another transport cycle (not shown). Finally, it is envisioned that specific transport receptors may be attached to the transporter in a side-specific manner, either transiently or as a permanent part of the structure.

nisms responsible for coordinating the specificity, timing, and directionality of transport will prove interesting.

I wish to thank the Division of Structural Studies at the Laboratory of Molecular Biology and P. N. T. Unwin for support and computing and my colleagues in the Department of Cell Biology at Stanford where the data were collected. Special thanks are due to Roger Lucke for construction of the perspex model and C. Toyoshima, D. Goldfarb, M. Rout, and P. N. T. Unwin for helpful discussions, Ildiko Virag for help with figures, and M. Radermacher, J. Carazo, and J. Frank for advice on the classification analysis.

This work was supported in part by a new investigator research award from the National Institutes of Health (R23-AM34164-02).

Received for publication 16 November 1989 and in final form 21 March 1990.

REFERENCES

Adams, S. A., T. J. Lobl, M. A. Mitchell, and L. Gerace. 1989. Identification of specific binding proteins for a nuclear localization sequence. *Nature (Lond.).* 337:276–279.

Aebi, U., J. Cohn, L. Buhle, and L. Gerace. 1986. The nuclear lamina is a meshwork of intermediate-type filaments. *Nature (Lond.)* 3232:560–564.

Akey, C. W. 1989*a*. Interactions and structure of the nuclear pore complex revealed by cryo-electron microscopy. *J. Cell Biol.* 109:955–970.

Akey, C. W. 1989*b*. A modular model of the nuclear pore complex. *Springer Ser. Biophys.* 3:307–311.

Akey, C. W., and D. S. Goldfarb. Protein import through the nuclear pore complex is a multi-step process. *J. Cell Biol.* 109:971–982.

Baglia, F. A., and G. G. Maul. 1983. Nuclear RNP release and nucleoside triphosphatase activity are inhibited by antibodies to a nuclear matrix glycoprotein. *Proc. Natl. Acad. Sci. USA.* 80:2285–2289.

Berrios, M., and P. A. Fisher. 1986. A myosin heavy chain-like polypeptide is associated with the nuclear envelope in higher eukaryotic cells. *J. Cell Biol.* 103:711–724.

Baker, T. S., J. Drak, and M. Bina. 1988. Reconstruction of the three-dimensional structure of simian virus 40 and visualization of the chromatin core. *Proc. Natl. Acad. Sci. USA.* 85:422–426.

Borer, R. A., C. F. Lehner, H. M. Eppenberger, and E. A. Nigg. 1989. Major nucleolar proteins shuttle between nucleus and cytoplasm. *Cell* 56:379–390.

Breeuwer, M., and D. S. Goldfarb. 1990. Facilitated nuclear transport of histone H1 and other small nucleophilic proteins. *Cell.* 60:999–1008.

Carazo, J. M., F. F. Rivera, E. L. Zapata, M. Radermacher, and J. Frank. 1990. Fuzzy sets-based classification of electron microscopy images of biological macromolecules with an application to ribosome particles. *J. Microsc.* 157:187–203.

Dabauvalle, M.-C., B. Schultz, U. Scheer, and R. Peters. 1988. Inhibition of nuclear accumulation of karyophilic proteins in living cells by microinjection of the lectin WGA. *Expl. Cell Res.* 174:291–296.

Davey, J., N. J. Dimnock, and A. Colman. 1985. Identification of the sequence responsible for the nuclear accumulation of the influenza virus nucleoprotein in *Xenopus* oocytes. *Cell.* 40:667–675.

Davis, L. I., and G. Blobel. 1986. Identification and characterization of a nuclear pore complex protein. *Cell* 45:699–709.

Dequin, R., H. Saumweber, and J. W. Sedat. 1984. Proteins shifting from the cytoplasm into the nuclei during early embryogenesis of *Drosophila* melanogaster. *Dev. Biol.* 104:37–48.

DeRobertis, E. M., R. E. Longthorne, and J. B. Gurdon. 1978. The intracellular migration of nuclear proteins in *Xenopus* oozytes. *Nature (Lond.).* 272:254–256.

Dingwall, C., and R. A. Laskey. 1986. Protein import into the cell nucleus. *Annu. Rev. Cell Biol.* 2:367–390.

Dingwall, C., S. V. Sharnick, and R. A. Laskey. 1982. A polypeptide domain that specifies migration of nucleoplasmin into the nucleus. *Cell* 30:449–458.

Dingwall, C., J. Robbins, S. M. Dilworth, B. Roberts, and W. C. Richardson. 1988. The nucleoplasmin nuclear localization sequence is larger and more complex than that of SV-40 large T antigen. *J. Cell Biol.* 107:841–849.

Dreyer, C., and P. Hausen. 1983. Two-dimensional gel analysis of the fate of oocyte nuclear proteins in the development of *Xenopus laevis*. *Dev. Biol.* 100:412–425.

Dworetzky, S. I., and C. M. Feldherr. 1988. Translocation of RNA-coated gold particles through the nuclear pores of oocytes. *J. Cell Biol.* 106:575–584.

Featherstone, C., M. Darby, and L. Gerace. 1988. A monoclonal against the nuclear pore complex inhibits nucleocytoplasmic transport of protein and RNA in vitro. *J. Cell Biol.* 107:1289–1297.

Feldherr, C. M., E. Kallenbach, and N. Schultz. 1984. Movement of a karyophillic protein through the nuclear pores of oocytes. *J. Cell Biol.* 99:2216–2222.

Finlay, D. R., and D. J. Forbes. 1990. Reconstitution of biochemically altered nuclear pore complexes: transport can be eliminated and restored. *Cell* 60:17–29.

Finlay, D. R., D. D. Newmeyer, T. M. Price, and D. J. Forbes. 1987. Inhibition of in vitro nuclear transport by a lectin that binds to nuclear pores. *J. Cell Biol.* 104:189–200.

Frank, J., J. P. Bretaudiere, J. M. Carazo, A. Verschoor, and T. Wagenknecht. 1988. Classification of images of biomolecular assemblies: a study of ribosomes and ribosomal subunits of *Escherichia coli*. *J. Microc.* 150:99–115.

Frank, J., B. Shimkin, and H. Dowse. 1981. SPIDER: a modular software system for electron image processing. *Ultramicrosc.* 6:343–358.

Franke, W. W. 1974. Structure, biochemistry and functions of the nuclear envelope. *Int. Rev. Cytol.* 4(Suppl.):71–236.

Gerace, L., and B. Burke. 1988. Functional organization of the nuclear envelope. *Annu. Rev. Cell Biol.* 4:335–374.

Hadjiolov, A. A. 1985. The Nucleolus and Ribosome Biogenesis. Springer-Verlag, New York.

Hendrix, R. W. 1978. Symmetry mismatch and DNA packaging in larger bacteriophage. *Proc. Natl. Acad. Sci. USA.* 75:4779–4783.

Hunt, T. 1989. Cytoplasmic anchoring proteins and the control of nuclear localization. *Cell* 59:949–951.

Kalderon, D., W. S. Richardson, A. F. Markham, and A. E. Smith. 1984. Sequence requirements for nuclear localizaiton of simian virus 40 large T-antigen. *Nature (Lond.).* 311:33–38.

Lawrence, J. B., R. H. Singer, and L. M. Marselle. 1989. Highly localized tracks of specific transcripts within interphase nuclei visualized by in situ hybridization. *Cell.* 57:493–502.

Mehlin, H., A. Lonnroth, U. Skoglund, and B. Daneholt. 1988. Structure and transport of a specific premessenger RNP particle. *In*

Nucleocytoplasmic Transport. R. Peters, editor. Academic Press, Inc., New York. 65–72.

Milligan, R. A. 1986. A structural model for the nuclear pore complex. *In* Nucleocytoplasmic Transport. R. Peters and M. Trendelenburg, editors. Springer-Verlag, New York. 113–122.

Milligan, R. A., and P. F. Flicker. 1987. Structural relationships of actin, myosin and tropomyosin revealed by cryoelectron microscopy. *J. Cell Biol.* 105:29–39.

Newmeyer, D. D., and D.J. Forbes. 1988. Nuclear import can be separated into distinct steps in vitro: nuclear pore binding and translocation. *Cell.* 52:641–653.

Newmeyer, D. D., J. M. Lucocq, T. R. Burglin, E. M. DeRobertis. 1986*a*. Assembly in vitro of nuclei active in nuclear protein transport: ATP is required for nucleoplasmin accumulation. *EMBO (Eur. Mol. Biol. Organ.) J.* 5:501–510.

Newmeyer, D. D., D. R. Finlay, and D. J. Forbes. 1986*b*. In vitro transport of a fluorescent nuclear protein and exclusion of non-nuclear proteins. *J. Cell Biol.* 103:2091–2102.Newport, J. W., and D. J. Forbes. 1987. The nucleus: structure, function and dynamics. *Annu. Rev. Biochem.* 56:535–565.

Newport, J. W., and D. J. Forbes. 1987. The nucleus: structure, function and dynamics. *Annu. Rev. Biochem.* 56:535–565.

Paine, P. L. 1975. Nucleocytoplasmic movement of fluorescent tracers microinjected into living salivary gland cells. *J. Cell Biol.* 66:652–657.

Paine, P. L., L. C. Moore, and S. B. Horowitz. 1975. Nuclear envelope permeability *Nature (Lond.).* 254:109–114.

Peters, R. 1984. Nucleocytoplasmic flux and intracellular mobility in single hepatocytes measured by fluorescence microphotolysis. *EMBO (Eur. Mol. Biol. Organ.) J.* 3:1831–1836.

Rayment, I., T. S. Baker, D. L. D. Caspar, and W. T. Murakami. 1982. Polyoma virus capsid structure at 22.5 angstroms resolution. *Nature (Lond.).* 295:110–115.

Reichelt, R., A. Holzenburg, E. L. Buhle, Jr., M. Jarnik, A. Englel, and U. Aebi. 1990. Correlation between structure and mass distribution of the nuclear pore complex and of distinct pore complex components. *J. Cell Biol.* 110:883–894.

Richardson, W. D., A. D. Mills, S. M. Dilworth, R. A. Laskey, and C. Dingwall. 1988. Nuclear protein migration involves two steps: rapid binding at the nuclear envelope followed by slower translocation through the nuclear pores. *Cell* 52:655–664.

Rihs, H.-P. and R. Peters. 1989. Nuclear transport kinetics depend on phosphorylation site containing sequences flanking the karyophilic signal of the Simian virus 40 T-antigen. *EMBO (Eur. Mol. Biol. Organ.) J.* 8:1479–1484.

Roth, S., D. Stein, and C. Nusslein-Volhard. 1989. A gradient of nuclear localization of the dorsal protein determines dorsoventral pattern in the *Drosophila* embryo. *Cell* 59:1189–1202.

Rushlow, C. A., K. Han, J. L. Manley, and M. Levine. 1989. The graded distribution of the dorsal morphogen is initiated by selective nuclear transport. *Cell* 59:1165–1177.

Scheer, U., M.-C. Dabauvalle, H. Merkert, and R. Benevente. 1988. The nuclear envelope and the organization of the nuclear pore complexes. *In* Nucleocytoplasmic Transport. Academic Press, Inc., New York. 5–25.

Servetnick, M. D., and F. H. Wilt. 1987. Changes in the synthesis and intracellular localization of nuclear proteins during embryogenesis in the sea urchin *Strongylocentrotus purpuratus. Dev. Biol.* 123:231–244.

Snow, C. M., A. Senior, and L. Gerace. 1987. Monoclonal antibodies identify a group of nuclear pore complex glycoproteins. *J. Cell Biol.* 104:1143–1156.

Stevens, B. J. and H. Swift. 1966. RNA transport from nucleus to cytoplasm in *Chironomus* salivary glands. *J. Cell Biol.* 31:55–77.

Steward, R. 1989. Relocalization of the dorsal protein from the cytoplasm to the nucleus correlates with its function. *Cell* 59:1179–1188.

Unwin, P. N. T., and R. A. Milligan. 1982. A large particle associated with the perimeter of the nuclear pore complex. *J. Cell Biol.* 93:63–75.

van Heel, M. 1987. Similarity measures between images. *Ultramicroscopy.* 21:95–100.

Wright, C. S. 1977. The crystal structure of wheat germ agglutinin at 2.2 angstroms resolution. *J. Mol. Biol.* 111:439–457.

Yoneda, Y., N. Imamoto-Sonobe, M. Yamaizumi, and T. Uchida, 1987. Reversible inhibition of protein import into the nucleus by wheat germ agglutinin injected into cultured cells. *Exp. Cell Res.* 173:586–595.

Zasloff, M. 1983. tRNA transport from the nucleus in a eukaryotic cell: a carrier-mediated translocation process. *Proc. Natl. Acad. Sci. USA.* 80:6436–6440.

Zeller, R., T. Nyffenegger, and E. M. DeRobertis. 1983. Nucleocytoplasmic distribution of snRNPs and stockpiled snRNA-binding proteins during oogenesis and early development in *Xenopus laevis. Cell* 32:425–434.